



# Prediction and experimental research of abrasive belt grinding residual stress for titanium alloy based on analytical method

Guijian Xiao<sup>1,2</sup> · Kangkang Song<sup>1</sup> · Yi He<sup>1</sup> · Wenxi Wang<sup>1,2</sup> · Youdong Zhang<sup>1</sup> · Wentao Dai<sup>1</sup>

Received: 8 August 2020 / Accepted: 10 May 2021 / Published online: 22 May 2021

© The Author(s), under exclusive licence to Springer-Verlag London Ltd., part of Springer Nature 2021

## Abstract

As an important material, titanium alloy is widely used in the manufacture of aircraft engine parts, and its processed surface quality is critical to the performance of aircraft engines. Abrasive belt grinding (ABG) is a kind of elastic grinding, which plays a significant role in improving titanium alloys' surface integrity. To validate the mathematical model's effectiveness from the grinding parameters to the surface residual stress after grinding, firstly, according to the molecular dynamics theory and ABG process, a physical model of titanium alloy ABG molecular system is proposed, and the embedded atom method is chosen as the interatomic potential of titanium alloy. Secondly, combined with the mathematical expression model of residual stress, the surface residual stress is characterized, and the heat correction coefficient is proposed to modify the mathematical model. Finally, based on molecular dynamics, the simulation of grinding residual stress and the grinding experiment is carried out for titanium alloy thin-walled parts. The results of simulation and experiment show that the trend of simulation results is similar to the experiment results. The simulation model can better represent the change rule of ABG surface residual stress for the titanium alloy material, but the average error rate is up to 15.01% due to the systematic error between the two. After correction, the average error rate between the simulation values and experiment values of residual stress on the surface decreases to 4.44%; the effectiveness of the mathematical model is verified.

**Keywords** Titanium alloy thin-walled parts · Abrasive belt grinding · Molecular dynamics · Mathematical model · Residual stress · VII

## 1 Introduction

With the unprecedented increase in demand for civil aerospace and military aerospace, the performance requirements of aeroengine materials are getting higher and higher. Titanium alloy, as a typical high-performance and difficult-to-machine material, is widely used in the manufacture of aeroengine blade [1, 2]. Previous research found that the surface residual stress after machining can easily lead to warpage and deformation of parts. It was also found that the surface residual stress has a great impact on the corrosion resistance, fatigue resistance, and other properties of parts [3–5]. In recent years, abrasive belt grinding (ABG) has been used for a wide range of the machining of titanium alloy complex curved surfaces and the control of surface residual stress because of its dual functions of grinding and polishing [6, 7]. Therefore, it is significant to detect and predict the surface residual stress accurately for guiding the design and processing of parts and improving the surface quality.

✉ Guijian Xiao  
xiaoguijian@cqu.edu.cn

Kangkang Song  
20190701143@cqu.edu.cn

Yi He  
heyi@cqu.edu.cn

Wenxi Wang  
wx.wang@cqu.edu.cn

Youdong Zhang  
13260537433@163.com

Wentao Dai  
daiwentao6666@163.com

<sup>1</sup> College of Mechanical Engineering, Chongqing University, No.174, Shazhengjie, Shapingba, Chongqing 400044, China

<sup>2</sup> The State Key Laboratory of Mechanical Transmissions, No.174, Shazhengjie, Shapingba, Chongqing 400044, China

To realize the prediction of surface residual stress, some scholars have researched it. Rami et al. [8] used three-dimensional (3D) simulation technology based on a hybrid method to evaluate the residual stress produced by the rolling and polishing process of AISI 4140 steel. The results showed that the established numerical model had better qualitative results for the residual stress under different polishing forces and feed speeds. Nikam and Jain [9] predicted the residual stress in the process of microplasma transfer arc using the finite element method (FEM). The simulation results indicated that the tensile residual stress at the junction of deposition and matrix is higher, and the tensile residual stress at the midpoint of the deposition path is the smallest. Wang et al. [10] established a finite element elastic-plastic contact model considering the hardness gradient and initial residual stress. The initial residual stress distribution was obtained by experimental measurement. Choi et al. [11] simulated the residual stress of the AA7085 rectangular steel bar by using ABAQUS/Standard software, compared the simulated residual stress with the experiment results of the longitudinal cutting method, and verified the accuracy of the model. Koňár and Patek [12] predicted the residual stress of the X5CrNi18-10/S355J2H welding joint using SYSWELD software, to prevent failure. Darmadi [13] predicted the residual stress of multi-pass girth weld by FEM. It was found that the prediction result of using the maraging model was closer to the experiment. Wang et al. [14] predicted the complete residual stress state of solid by using the data of surface stress measurement and proposed a FEM. The experiment results indicated that the method could predict the residual stress field well.

The above research mainly focuses on predicting residual stress by finite element simulation, while other scholars put forward the prediction of residual stress based on the analytical method. Sun et al. [15] proposed a new residual stress prediction model that comprehensively considers the dynamic characteristics, mechanical-heat coupling, and deformation effects. Based on the above factors, the multiphase field's residual stress was established, and the results were in good agreement with the results of the dynamic grinding hardening experiment. Valíček et al. [16] predicted the residual stress distribution after milling by putting forward an analytical method. The results indicated that the strength of residual stress is determined by the roughness and its control. The theoretical calculation results and experiment results agree well with the results of the literature investigation, which proves the validity of this method. Lu et al. [17] proposed a grain size sensitive-MTS model. The analysis results were compared with the experimental research and the classical Johnson-Cook model, which verified the model's effectiveness in residual stress prediction. Pan et al. [18] proposed a prediction and analysis model of orthogonal turning residual stress considering thermal effect. The predicted residual stress was very close to the measured values. Fergani et al. [19] proposed various

prediction models for the residual stress of single pass martensite. The results showed that the test data of the AA2121-T3 milling process agree well with the model prediction. Zheng et al. [20] proposed a model to predict the residual stress distribution after riveting. Combined with the residual stress calculated by the model, the fatigue life was predicted using the multiaxial fatigue criterion. Shan et al. [21] proposed a residual stress prediction model based on an analytical method considering mechanical stress and thermal stress in the orthogonal cutting process. Through the orthogonal cutting experiment of a pipeline, the validity of the proposed residual stress prediction method was verified.

In addition, Ling et al. [22] gave the longitudinal stress distribution of the linear guide during the straightening process and the numerical calculation method of the straightening stroke considering the residual stress inheritance characteristics. The results showed that the compressive residual stress generated during the straightening process leads to the compressive residual stress after grinding. Doan et al. [23] simulated the residual stress of Cu-Zr metal film by using molecular dynamics. When the indentation force values is 100~185 nN, the residual stress value is 0.44~0.82 GPa in the loading stage and 0.4~0.9 GPa in the unloading stage.

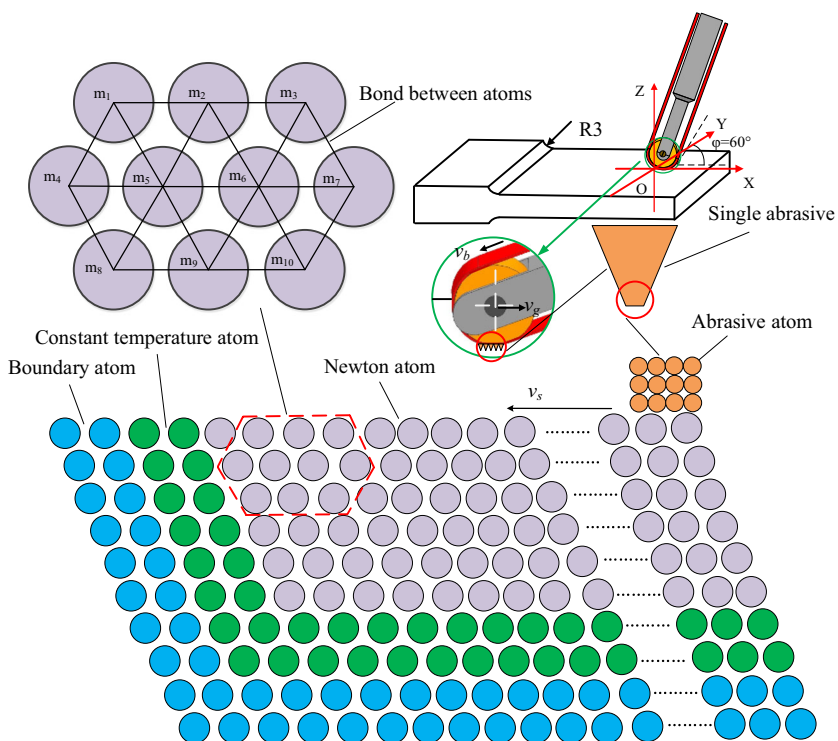
In conclusion, there are many studies on residual stress prediction, which mainly focus on the prediction of milling, turning, and welding. However, there are few reports on the prediction of ABG residual stress of titanium alloy thin-walled parts by using molecular dynamics. Therefore, this study chooses the residual stress on the ABG surface as the research object. The established mechanical model is calculated by molecular dynamics, the mathematical model from ABG parameters to surface residual stress is obtained, and the characterization of surface residual stress is realized. The effectiveness and accuracy are verified by comparing simulation results with the experiment results of ABG of titanium alloy thin-walled parts.

## 2 Molecular dynamics analysis of titanium alloy ABG

### 2.1 Establishment of physical model of molecular system for titanium alloy ABG

In the actual ABG process, because the size of ABG particles is much larger than the size of the molecular system of parts to be processed, the actual contact between ABG particles and parts to be processed is surface contact, so the ABG particles can be abstracted as a cube in the model. The ABG process of titanium alloy thin-walled part is abstracted as a physical model divided into Newton atom, constant temperature atom, and boundary atom, as shown in Fig. 1. In Fig. 1, the Newton atom is affected by ABG particles. In molecular dynamics system,

**Fig. 1** Molecular system of ABG on titanium alloy surface



its motion law conforms to Newton’s law of motion. Although the constant temperature atom is affected by the Newton atom, its energy will not change. The boundary atom is an atom that is not affected by the ABG particle’s action. Combined with molecular system dynamics, the stress between particles is analyzed by delamination and recombination under the action of external force; the characterization of residual stress is realized.

Because the titanium alloy molecular system can be regarded as a 3D model, the established traditional Cartesian coordinate system is used to express the molecular kinematic vectors that will result in a lot of complicated calculations. Therefore, this study converts the 3D molecular model into a planar two-dimensional molecular model system and considers the residual stress generated by the molecular system’s movement in the plane *x* and *y* direction. In addition, the grinding feed speed, abrasive belt speed, and grinding pressure in the grinding process are all transformed into the speed change of the system by Newton motion.

Because the basic theory of molecular system dynamics is Newton’s law of motion, the parameters of the molecular system can be obtained by differential equations and computer calculations. Therefore, the molecular motion calculated by quantum mechanics will not be considered in the subsequent simulation. In this way, we can get the any molecule force in the system according to the potential energy function.

$$\vec{F}_i = -\nabla_i U = -\left(\vec{i} \frac{\partial}{\partial x_i} + \vec{j} \frac{\partial}{\partial y_i} + \vec{k} \frac{\partial}{\partial z_i}\right) \quad (1)$$

According to Newton’s second law, the acceleration of titanium alloy molecule *i* can be calculated.

$$\vec{a}_i = \frac{\vec{F}_i}{m_i} \quad (2)$$

In the ideal model of molecular crystal, molecules are arranged repeatedly in 3D space. Different metals have different crystal structures. The research object of this paper is the grinding process of titanium alloy. Titanium is used as the metal-solvent, and other metals are incorporated into the crystal lattice of titanium to form a solid solution titanium alloy. Titanium crystal is a hexagonal close-packed (HCP) structure, so the titanium alloy formed is an HCP structure.

### 2.2 Establishment of mathematical model of molecular system for titanium alloy ABG

The selection of intermolecular potential function directly affects the accuracy of the subsequent model establishment of the molecular system. At present, the intermolecular potential function widely used mainly includes the pair potential model and the multi-body potential model. The pair potential model has a large error when it is used to simulate the changes of the metal compound molecular system, and the multi-body potential model can avoid this problem. In the multi-body potential energy model, according to the functional method and the molecular distribution density, the embedded atom method (EAM) is developed. The following hypothesis is put forward:

the electron density of metal molecular system can be linearly superposed by each electron at a certain place. In the EAM model, a molecule embedded in the molecular system is separated as an atom embedded in the molecular system, and then the interaction between other atoms is called the embedded energy. EAM considers the interaction between atoms and the embedded energy of molecular system.

In EAM, the total energy of titanium alloy molecular system is as follows:

$$\begin{cases} E = \frac{1}{2} \sum_{i,j,i \neq j} \phi(r_{ij}) + \sum_i F_i(\rho_i) \\ \rho_i = \sum_{i,j,i \neq j} f_i(r_{ij}) \end{cases} \quad (3)$$

where  $E$  is the total energy of molecular system;  $\phi$  is the two-body interaction potential of molecular system;  $F_i$  is the molecular embedded energy of molecular system;  $\rho_i$  is the electron density at molecule  $i$ ;  $f_i(r_{ij})$  is the electron density generated by molecule  $j$  at molecule  $i$  with distance  $r_{ij}$ ;  $r_{ij}$  is the distance between molecule  $i$  and molecule  $j$ . Here,  $F_i(\rho_i)$  and  $\rho_i$  satisfy the functional relationship.

Zhou et al. [24] gave the expressions of  $f(r)$  and  $\phi(r)$ :

$$f(r) = \frac{f_e \exp\left[-\beta\left(\frac{r}{r_e}-1\right)\right]}{1 + \left(\frac{r}{r_e}-\lambda\right)^{20}} \quad (4)$$

$$\phi(r) = \frac{A \exp\left[-\alpha\left(\frac{r}{r_e}-1\right)\right]}{1 + \left(\frac{r}{r_e}-\kappa\right)^{20}} - \frac{B \exp\left[-\beta\left(\frac{r}{r_e}-1\right)\right]}{1 + \left(\frac{r}{r_e}-\lambda\right)^{20}} \quad (5)$$

where  $A$ ,  $B$ ,  $\alpha$ , and  $\beta$  are variable parameters;  $\kappa$  and  $\lambda$  are intercept parameters;  $r_e$  is the equilibrium distance of the nearest particles.

The expression of embedded energy is:

$$\begin{cases} F(\rho) = \sum_{i=0}^3 F_{ni} \left(\frac{\rho}{0.85\rho_e}-1\right)^i & \rho < 0.85\rho_e \\ F(\rho) = \sum_{i=0}^3 F_i \left(\frac{\rho}{\rho_e}-1\right)^i & 0.85\rho_e \leq \rho < 1.15\rho_e \\ F(\rho) = F_e \left[1 - \ln\left(\frac{\rho}{\rho_e}\right)\right]^\eta \left(\frac{\rho}{\rho_e}\right)^\eta & 1.15\rho_e \leq \rho \end{cases} \quad (6)$$

where  $\rho_e$  is the equilibrium electron density;  $\rho$  is the electron density.

In Table 1, part of the physical parameters required for establishing EAM potential function of titanium alloy is listed.

The force state and acceleration of each molecule can be obtained from the energy gradient, and the molecular coordinates and velocities after a certain number of cycle steps can

**Table 1** Physical parameters of EAM potential function of titanium alloy [24]

| Parameters | $r_e$    | $f_e$    | $\kappa$  | $\alpha$  | $\beta$  |
|------------|----------|----------|-----------|-----------|----------|
| Value      | 2.933872 | 1.863200 | 0.5       | 8.775431  | 4.680230 |
| Parameters | $A$      | $B$      | $\lambda$ | $\rho$    | $\mu$    |
| Value      | 0.373601 | 0.570968 | 1.0       | 25.565138 | 0.558572 |

be obtained by combining the leap-frog algorithm. Because the derivation of traditional hydrodynamics residual stress is based on the model derived everywhere and continuously, it is crucial to choose the appropriate formula of ABG residual stress of titanium alloy. According to Zhou [25], the virial stress of a single atom is:

$$\sigma_i = \left( -m_i v_i^m v_i^n + \frac{1}{2} \sum_{i,j,i \neq j} F_{ij} r_{ij} \right) / V_i \quad (7)$$

where  $\sigma_i$  is the residual stress of atom  $i$ ;  $m_i$  is the mass of atom  $i$ ;  $V_i$  is the volume of the atom  $i$ ,  $V_i = \frac{4\pi a_i^3}{3}$ , and  $a_i = \frac{\sum_j r_{ij}^{-1}}{2 \sum_j r_{ij}^{-2}}$ ;

$v_i^m, v_i^n$  are the speed component of atom  $i$  in horizontal and vertical directions;  $N$  is the number of atoms in the system;  $F_{ij}$  is the force of atom  $i$  from atom  $j$ ,  $F_{ij} = \frac{\partial \phi(r_{ij})}{\partial r_{ij}}$ ,  $\phi(r_{ij})$  is the potential energy of an atom;  $r_{ij}$  is the distance vector between atom  $i$  and atom  $j$ .

To establish the mathematical model from grinding parameters to surface residual stress, it is necessary to introduce the expression from grinding parameters to grinding force:

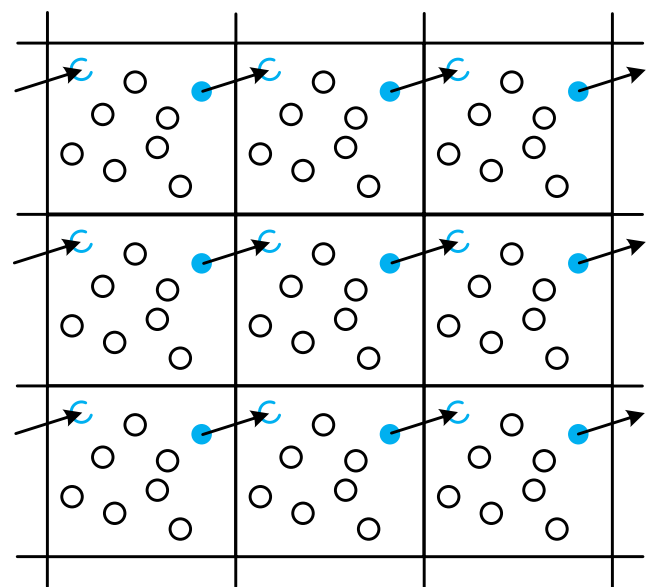
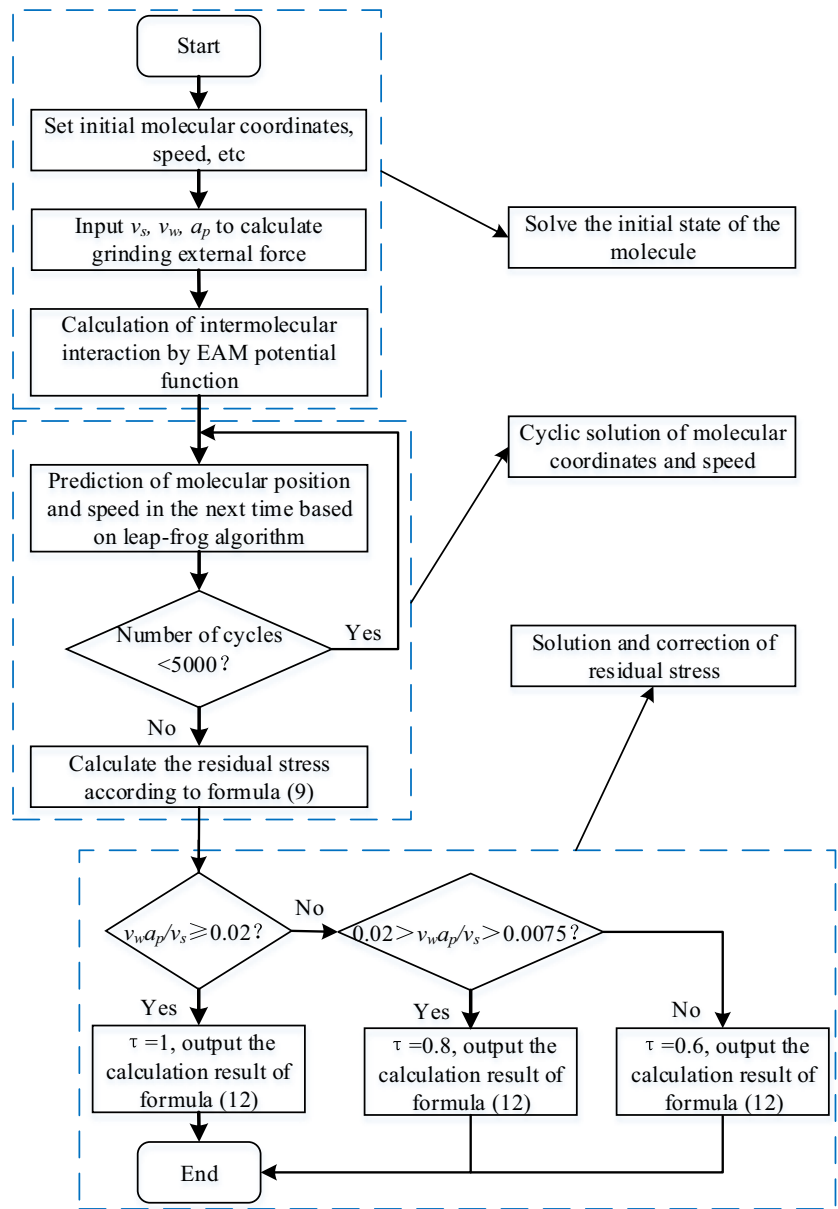


**Fig. 2** Boundary conditions of molecular system simulation

Fig. 3 MATLAB simulation flow chart



$$\begin{cases} F_t = U_s \frac{v_w^{0.84}}{v_s} a_p^{0.71} B(1 + Z_s t) \\ F_n = U_s \frac{v_w^{0.84}}{v_s^{1.15}} a_p^{0.68} B(1 + Z_s t) \end{cases} \quad (8)$$

where  $F_t$  is the tangential predicted grinding force;  $F_n$  is the normal predicted grinding force;  $U_s$  is specific grinding energy, and its value varies according to different materials;  $a_p$  is the grinding depth;  $v_s$  is the abrasive belt speed;  $v_w$  is the workpiece feed speed;  $B$  is the abrasive belt width;  $Z_s$  is according to different ABG particles and grinding parameters; the range is  $2 \times 10^{-2} \sim 5 \times 10^{-5} \text{ s}^{-1}$ .

Because the states of the atoms in the system are different, the surface residual stress can be obtained by the average value of the atomic virial stress.

$$\sigma = \frac{\omega}{N} \sum_{i \in S} \left[ \left( -m_i v_i^m v_i^n + \frac{1}{2} \sum_{i,j,i \neq j} F_{ij} r_{ij} \right) / V_i \right] \quad (9)$$

where  $\omega$  is the shape correction coefficient, which can be measured by experiment. When the workpiece is a flat plate,  $\omega = 1$ .

In order to simplify the calculation, this paper takes Newtonian mechanics as the main basis of microcomputation and does not consider the influence of heat in the calculation process, so the calculation result of residual stress will have a large error. Zhang et al. [26] proposed the expression of grinding heat distribution ratio of ABG:

$$\varepsilon = \left( 1 - \frac{b a_p v_w e_w}{F_t v_s} \right) \times \frac{1}{1 + \frac{0.97 k_g}{\sqrt{r_0 v_s (k \rho c)_w}}} \quad (10)$$

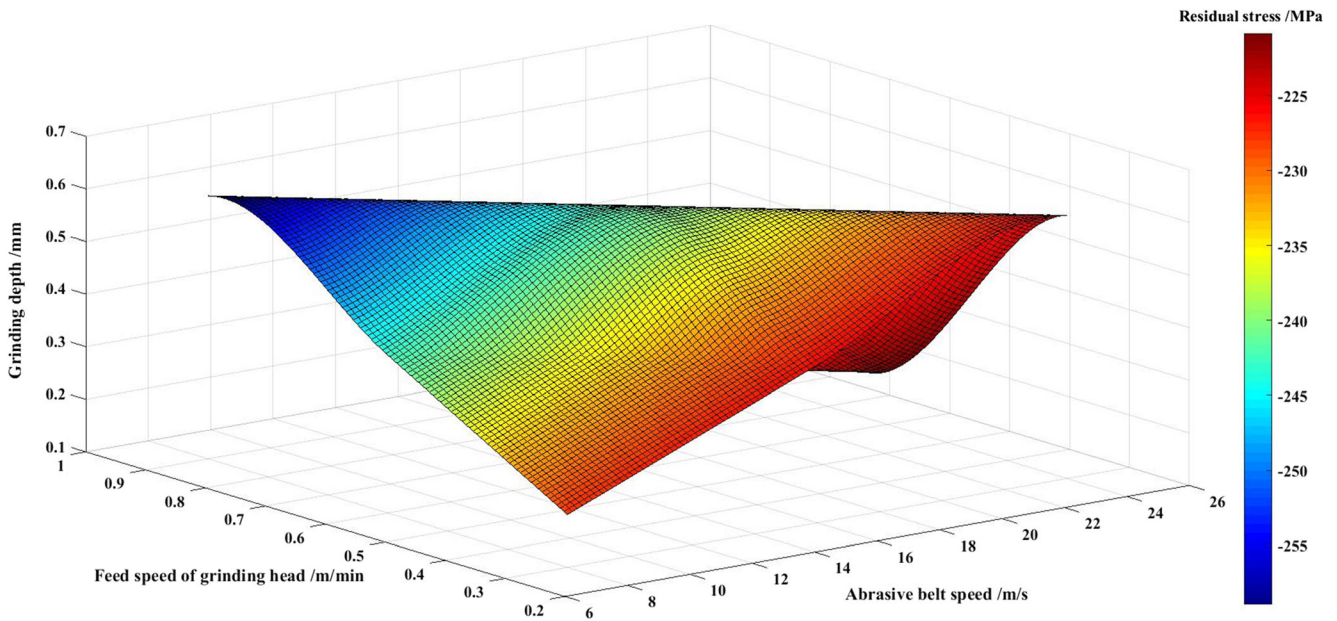


Fig. 4 Simulation results of ABG residual stress of titanium alloy

It can be seen that the heat allocated to the workpiece in the ABG process is negatively related to  $v_w \frac{a_p}{v_s}$ , that is, the magnitude of residual pressure stress is negatively related to  $v_w \frac{a_p}{v_s}$ . Therefore, the influence of heat is introduced into the simulation process. By changing different grinding parameters and combining with a lot of experiments, the heat correction coefficient  $\tau$  is proposed, which is defined as:

$$\tau = \begin{cases} 1 & \frac{v_w a_p}{v_s} \geq 0.02 \\ 0.8 & 0.02 > \frac{v_w a_p}{v_s} \geq 0.0075 \\ 0.6 & 0 < \frac{v_w a_p}{v_s} < 0.0075 \end{cases} \quad (11)$$

When formula (11) is introduced into formula (9), the corrected residual stress formula is as follows:

$$\sigma = \frac{\tau}{N} \sum_{i \in S} \left[ \left( -m_i v_i^m v_i^n + \frac{1}{2} \sum_{i,j,i \neq j} F_{ij} r_{ij} \right) / V_i \right] \quad (12)$$

### 3 Simulation of ABG residual stress of titanium alloy based on molecular dynamics

#### 3.1 Initial condition setting of molecular dynamics simulation

##### (1) Time step

Because the calculation of molecular system involves many physical quantities and cycle calculations, it is necessary to choose a reasonable time step to avoid too long simulation time. MATLAB software is developed based on C++ language. Compared with general C language software, the speed of non-vector loop operation is much slower. Therefore, the selected time step of system operation simulation is  $\Delta t = 1 \times 10^{-15} s$ .

Table 2 Parameters of each axis of the grinder

| Category  | Parameters          |
|---|---------------------|
| X, Y, Z axis positioning accuracy (mm)          | 0.012, 0.01, 0.01   |
| X, Y, Z axis repeated positioning accuracy (mm) | 0.008, 0.005, 0.005 |
| X, Y, Z feed speed (m/min)                      | 0~15                |



Fig. 5 Experimental platform of seven-axis six-linkage adaptive CNC abrasive belt grinder

(2) Boundary conditions of molecular system simulation

Because of the limited computing power of computer, the model of molecular dynamics simulation cannot be built completely according to the actual situation, only for a small area. However, because the system that can be simulated is too small, it is often far less than the material’s thermodynamic limit, which will produce size effect. Therefore, the periodic boundary conditions are introduced to achieve the correction. Periodic boundary condition is to divide the whole molecular system into many boxes. The number, distribution, and energy of particles in each box are identical, as shown in Fig. 2. When a particle leaves one side of the box, there must be a same particle entering the box at the same speed from the opposite side of the box. As a result, the total number of particles inside the box remains the same. After introducing periodic boundary conditions, each box state is completely equivalent. Therefore, only one box needs to be calculated and analyzed. Its states can be extended to the whole particle system to eliminate the size effect and reduce the calculation amount of simulation.

(3) Molecular system parameter simulation algorithm

Generally speaking, the Newton equation of multi-particle system cannot be solved analytically, so it needs to be solved by numerical integration method. In molecular dynamics, the Newton equation can be solved by the finite difference method. At a certain time, the external force of a particle is equal to the vector sum of all other particles’ forces on the particle. According to the particle’s force state, the acceleration of the particle at this time can be obtained. In the time step, the force is determined as a constant. Combined with the particle’s position and speed at this time, the position and speed of the next time can be obtained. Then, according to the new speed and position of the particles, we can get the new state of force, so repeatedly.

In this study, the leap-frog algorithm is adopted, and the speeds  $\vec{v}_i(t + \frac{\Delta t}{2})$  and  $\vec{v}_i(t - \frac{\Delta t}{2})$  are Taylor expanded at time  $t$ , respectively.

$$\vec{v}_i(t + \frac{\Delta t}{2}) = \vec{v}_i(t) + \vec{a}_i(t)(\frac{\Delta t}{2}) + \frac{1}{2!} \vec{b}_i(t)(\frac{\Delta t}{2})^2 + O(\Delta t^3) \quad (13)$$

$$\vec{v}_i(t - \frac{\Delta t}{2}) = \vec{v}_i(t) + \vec{a}_i(t)(-\frac{\Delta t}{2}) + \frac{1}{2!} \vec{b}_i(t)(-\frac{\Delta t}{2})^2 + O(\Delta t^3) \quad (14)$$

The subtraction of formula (13) and formula (14) can approximate all molecules’ speed of in the molecular system.

$$\vec{v}_i(t + \frac{\Delta t}{2}) - \vec{v}_i(t - \frac{\Delta t}{2}) = \vec{a}_i(t)(\Delta t) + O(\Delta t^3) \quad (15)$$

where  $O(\Delta t^3)$  is the higher order term of Taylor expansion, which can be ignored.

In the same way,  $\vec{r}_i(t + \Delta t)$  and  $\vec{r}_i(t)$  are expanded and sorted by Taylor at time  $t + \frac{\Delta t}{2}$ , and all molecules’ positions in the molecular system can be approximated.

$$\vec{r}_i(t + \Delta t) - \vec{r}_i(t) = \vec{v}_i(t + \frac{\Delta t}{2})(\Delta t) + O(\Delta t^3) \quad (16)$$

### 3.2 Molecular dynamics simulation process

According to the above algorithm and the established model, a MATLAB program is developed to simulate and analyze the surface residual stress for the molecular system. The simulation process is as follows:

(1) Set initial conditions

Combined with the simulated HCP structure of the molecular system on the titanium alloy surface, the molecular random speed is set. The coordinates of each atom will automatically deviate from the initial position as the system evolves.

(2) Exert external influence

According to the abrasive belt speed  $v_s$ , grinding head feed speed  $v_w$  and grinding depth  $a_p$  can be used to calculate the external force of ABG. Since the size of ABG particles is much larger than that of the molecular system, the external force can be set as uniform distribution.

(3) Calculate intermolecular influence

The intermolecular interaction is mainly determined by a potential function. In this study, according to the titanium alloy materials’ characteristics, EAM potential function is selected, and the intermolecular interaction can be calculated based on it.



Fig. 6 TC4 titanium alloy plate

**Table 3** Chemical element content of the test piece

| Element       | Al      | V       | Fe   | C    |
|---------------|---------|---------|------|------|
| Content (wt%) | 5.5~6.8 | 3.5~4.5 | ≤0.3 | ≤0.1 |
| Element       | N       | H       | O    | Ti   |
| Content (wt%) | ≤0.05   | ≤0.015  | ≤0.2 | bal  |

- (4) Prediction of molecular position and speed in the next time based on the algorithm

The algorithm selected in this study is leap-frog algorithm, which has high accuracy. According to this algorithm, the molecular position and speed can be predicted at the next moment.

- (5) Calculate molecular residual stress

When the number of cycles is more than 5000, the residual stress can be obtained by taking the molecular position and speed into formula (9) and formula (12).

The MATLAB simulation process is shown in Fig. 3.

### 3.3 Molecular dynamics simulation results

Figure 4 shows the simulation results of ABG residual stress of titanium alloy. In Fig. 4, the range of residual stress is from  $-220$  to  $-260$  MPa. Compared with the experiment results in Fig. 9, the trend is almost the same, but the difference of residual stress results under the grinding parameters is large.

## 4 ABG experiment of titanium alloy thin-walled parts

### 4.1 Experimental equipment

In this experiment, a new type of the seven-axis six-linkage adaptive CNC abrasive belt grinder is adopted. The grinder is controlled by an advanced CNC system and can be used for rough grinding, fine grinding, and automatic polishing of the workpiece surface, as shown in Fig. 5. Because the contact wheel itself has certain elasticity in the ABG process and the machine tool has a certain range of elastic movement in the Z-axis direction, the machine tool can realize flexible grinding in

**Table 4** Mechanical parameter values of the test piece

| Elasticity modulus (GPa) | Density (kg/m <sup>3</sup> ) | Yield strength (MPa) | Tensile strength (MPa) |
|--------------------------|------------------------------|----------------------|------------------------|
| 111.5                    | 4640                         | 1110                 | ≥895                   |

the machining process, greatly reducing the precision error brought by the small displacement of grinding head in the ABG process. The parameters of each axis of the grinder are listed in Table 2.

The test piece used in the experiment is TC4 (Ti-6Al-4V) titanium alloy plate, as shown in Fig. 6. The dimension is  $170 \times 100 \times 2$  (length  $\times$  width  $\times$  thickness) mm. The chemical element content and mechanical parameter values of the TC4 test piece at room temperature are listed in Table 3 and Table 4, respectively.

XK870F ceramic alumina abrasive belt of VSM company in Germany is selected, abrasive belt size is  $2540 \text{ mm} \times 5 \text{ mm}$ , and granularity is P240#. To detect the surface residual stress of the TC4 plate after processing, the  $\mu$ -X360s type stress meter of Japan Pulstec company is selected. The equipment can detect the non-destructive residual stress of the processed parts, and the measurement accuracy parameters are listed in Table 5.

### 4.2 Experimental method

The purpose of this experiment is to research the surface residual stress distribution characteristics of titanium alloy thin-walled parts after grinding and to explore the influence of grinding parameters on the surface residual stress value. The experimental grinding method is down grinding and dry grinding. The reciprocating grinding scheme is adopted, and the angle between the ABG head and the workpiece plane is  $60^\circ$ , as shown in Fig. 7.

Titanium alloy thin-walled parts have the characteristics of thin-walled weak stiffness, which is very easy to produce deformation in the process of machining, which will seriously affect the machining accuracy and surface integrity after machining, and finally lead to the decline of fatigue strength of parts. To reduce the deformation of titanium alloy caused by grinding force during grinding, the error correction technology is used to reduce the machining error. In the ABG process, the deformation is estimated or measured in advance, and then the tool path in the machining process is corrected to realize the correction of the error.

To realize the research on the main influence law of the ABG residual stress under the condition of less experimental

**Table 5** Measurement parameters of  $\mu$ -X360s type stress meter

| Category                        | Parameters                     |
|---------------------------------|--------------------------------|
| Systematic error                | $\pm 5$ MPa                    |
| Measuring speed                 | 2–3 min/point                  |
| Detection object                | Normal stress and shear stress |
| Minimum collimator              | $\leq 0.3$ mm                  |
| External signal touch interface | Open                           |





Fig. 7 ABG experiment of titanium alloy thin-walled parts

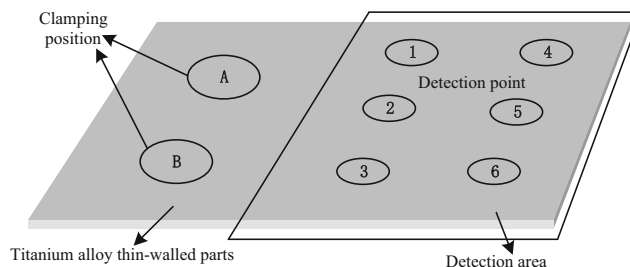


Fig. 8 Clamping position and detection point distribution

By detecting the residual stress of the processed part surface under different ABG parameters such as the  $v_s$ , the  $v_w$ , and the  $a_p$ , compared with the simulation results, the simulation results are verified to be correct.

times, this study uses the multi-factor orthogonal experimental method to design the experimental scheme. The effects of the abrasive belt speed, the feed speed of grinding head, and the grinding depth on the surface residual stress are comprehensively studied. Take 3 levels for each factor, and makeup 3 factors 3 level orthogonal experiment. The ABG parameters' setting is listed in Table 6.

The  $v_s$  can be obtained by formula (17).

$$v_s = \frac{\pi Dn}{60 \times 1000} \tag{17}$$

where  $D$  is the diameter of the drive wheel;  $n$  is the speed of the abrasive belt drive wheel.

The  $v_w$  and the  $a_p$  can be achieved by setting the grinding machine parameters during programming.

He et al. [27] proposed that the residual stress at the depth of 1.2  $\mu\text{m}$  is the largest after ABG; the selected detection depth is 1.2  $\mu\text{m}$ . To reduce the impact of random errors, detection points (1–6) are selected on the parts to be processed surface, and the experiment result is obtained by the measured average values of these six points. The clamping position and the distribution of detection points are shown in Fig. 8.

### 4.3 Experimental result

The ABG experiment results of titanium alloy thin-walled parts are depicted in Fig. 9. In Fig. 9, the range of residual stress in the experiment is from  $-150$  to  $-270$  MPa.

## 5 Simulation and experiment results analysis of titanium alloy ABG

### 5.1 Comparative analysis of simulation and experiment results before correction

- (1) Analysis of the relationship between residual stress and abrasive belt speed

The residual stress on the surface before correction is arranged according to the abrasive belt speed is depicted in Fig. 10, and the other corresponding grinding parameter settings are listed in Table 6. In Fig. 10, with the increase of the abrasive belt speed, the results of simulation before correction and experiment show a slow decline trend as a whole. However, most of the simulation results before the correction are larger

Table 6 ABG parameter setting

| Experiment number | Abrasive belt speed $v_s$ (m/s) | Feed speed of grinding head $v_w$ (m/min) | Grinding depth $a_p$ (mm) |
|-------------------|---------------------------------|---|---------------------------|
| 1                 | 8                               | 0.3                                       | 0.2                       |
| 2                 | 8                               | 0.6                                       | 0.4                       |
| 3                 | 8                               | 0.9                                       | 0.6                       |
| 4                 | 16                              | 0.3                                       | 0.4                       |
| 5                 | 16                              | 0.6                                       | 0.6                       |
| 6                 | 16                              | 0.9                                       | 0.2                       |
| 7                 | 24                              | 0.3                                       | 0.6                       |
| 8                 | 24                              | 0.6                                       | 0.2                       |
| 9                 | 24                              | 0.9                                       | 0.4                       |

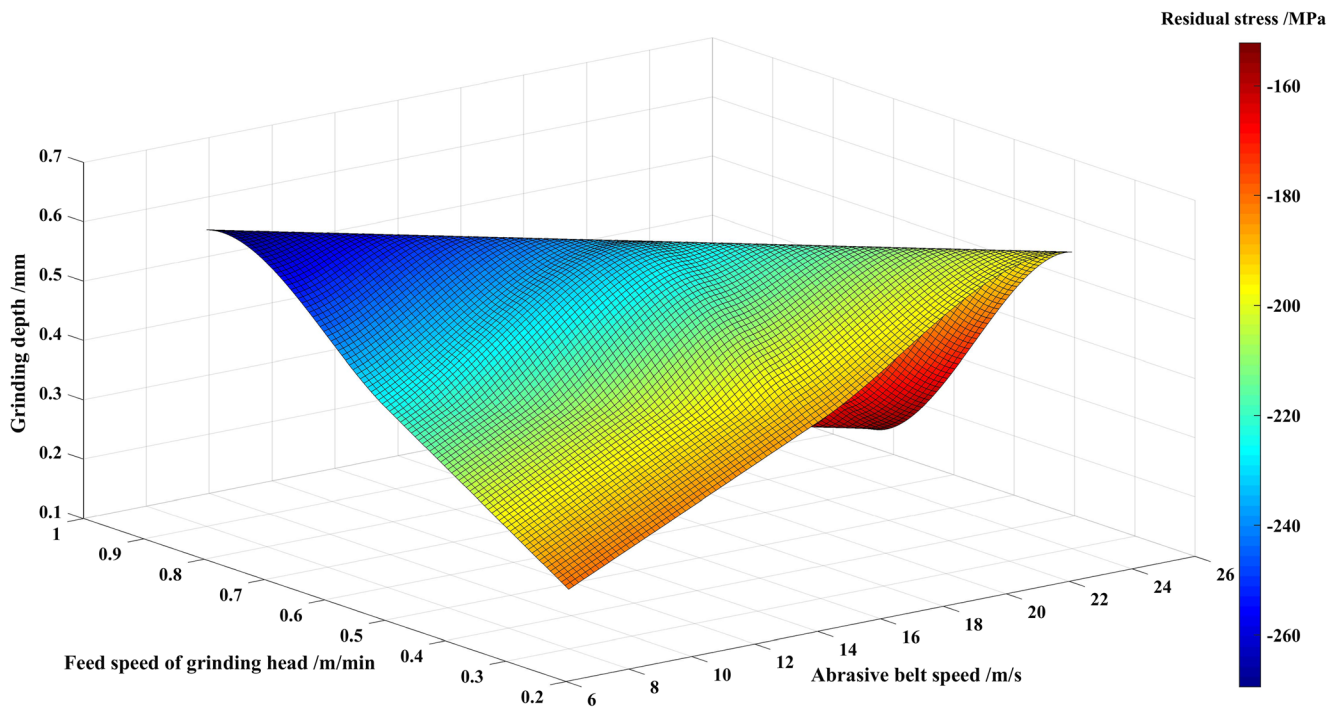


Fig. 9 ABG experiment results of titanium alloy thin-walled parts

than the experiment results, and the results of simulation and experiment before correction are quite different.

(2) Analysis of the relationship between residual stress and feed speed of grinding head

The surface residual stress before the correction is arranged based on the grinding head’s feed speed is depicted in Fig. 11, and the other corresponding grinding parameter settings are listed in Table 6. In Fig. 11, with the increase of grinding head’s feed speed, the results of simulation and experiment before correction show a slow increase trend as a whole. However, most of the simulation results before correction are larger than the experiment results, and the results of simulation and experiment before correction are quite different.

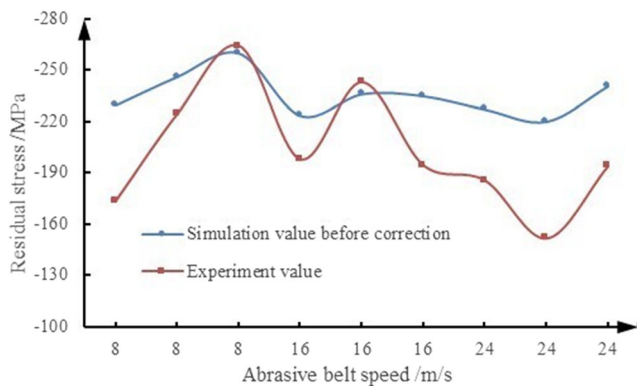


Fig. 10 Relationship between residual stress and abrasive belt speed before correction

(3) Analysis of the relationship between residual stress and grinding depth

The surface residual stress before correction is arranged based on the grinding depth is depicted in Fig. 12, and the other corresponding grinding parameter settings are listed in Table 6. In Fig. 12, with the increase of grinding depth, the simulation and experiment results before correction show a slow increasing trend as a whole, which are consistent. However, most of the simulation results before correction are larger than the experiment results, and the results of simulation and experiment before correction are quite different.

Through the above comparison, it can be found that the simulation results before correction are quite different from the experiment results, and the maximum residual stress error

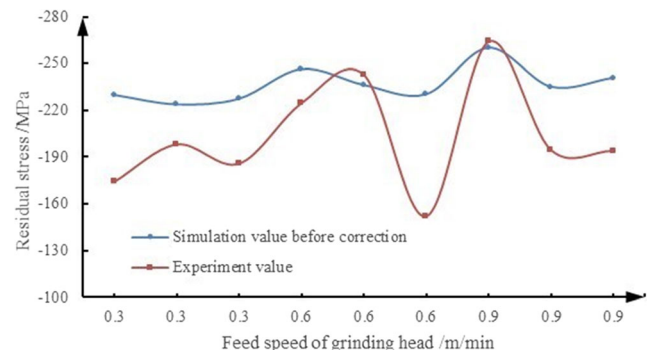
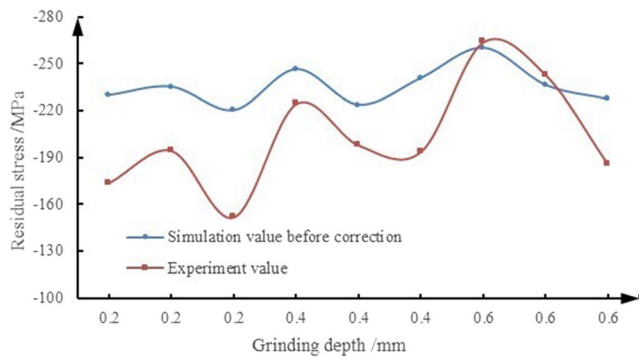


Fig. 11 Relationship between residual stress and feed speed of grinding head before correction



**Fig. 12** Relationship between residual stress and grinding depth before correction

is about 70 MPa. The above results may be that only grinding parameters are considered in the calculation of external forces in the simulation model before correction, and the influence of heat on the simulation results is ignored, resulting in a large error. Therefore, the influence of heat on the simulation results needs to be considered. According to the corrected formula (12), the residual stress considering the heat factor can be obtained.

### 5.2 Comparative analysis of simulation and experiment results after correction

The simulation results of the residual stress after correction are depicted in Fig. 13. In Fig. 13, the range of the residual stress after correction is from -150 to -270 MPa. Compared with the

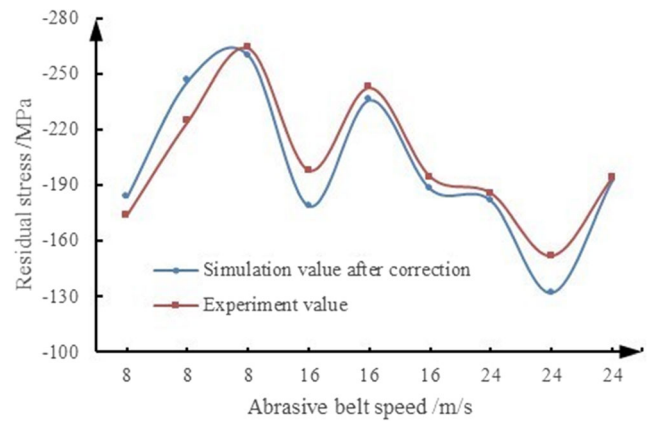


**Fig. 14** Relationship between residual stress and abrasive belt speed after correction

experiment results in Fig. 9, the trend is consistent, and the results of residual stress under the same grinding parameters are similar.

- (1) Analysis of the relationship between residual stress and abrasive belt speed

The residual stress on the surface after correction is arranged according to the abrasive belt speed is depicted in Fig. 14, and the other corresponding grinding parameter settings are listed in Table 6. In Fig. 14, with the increase of the abrasive belt speed, the surface residual stress decreases slowly. The fitting degree of the simulation curve and the experimental curve is higher after correction.

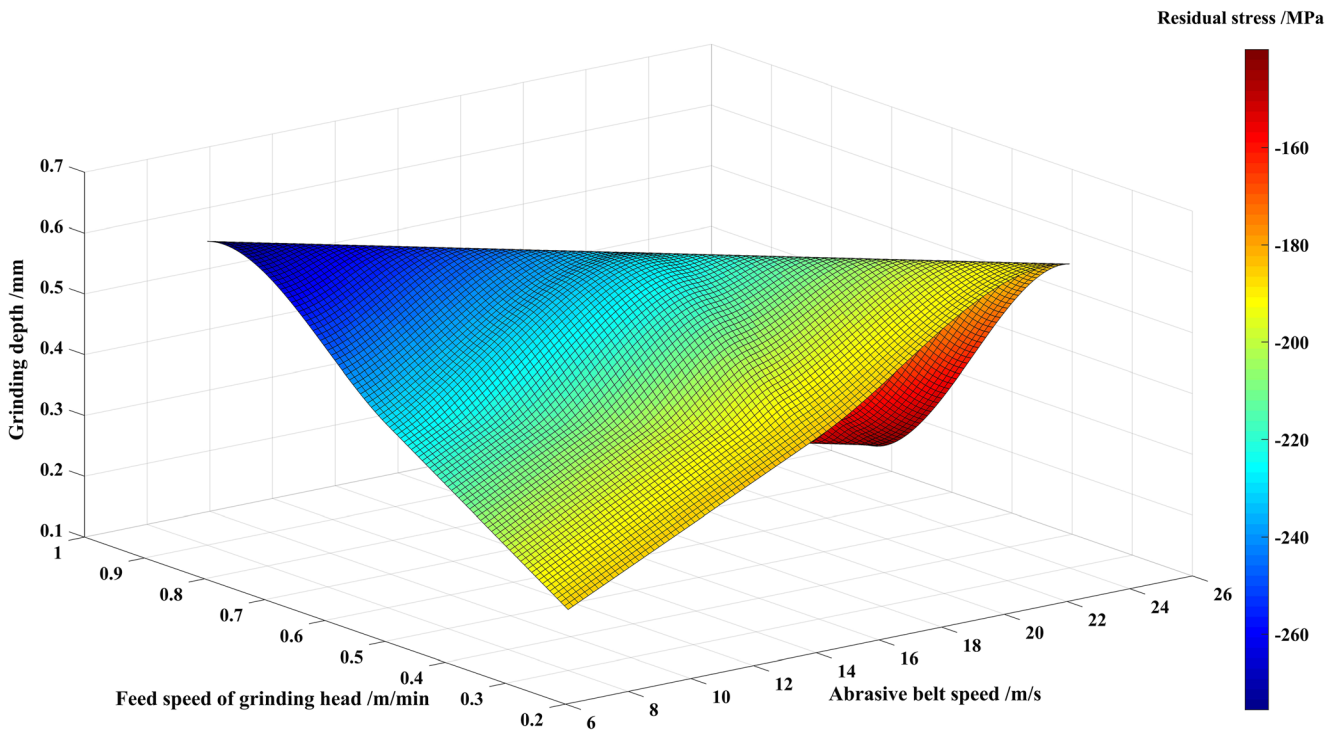


**Fig. 13** Simulation results of ABG residual stress of titanium alloy after correction

- (2) Analysis of the relationship between residual stress and feed speed of grinding head

The surface residual stress after the correction is arranged based on the grinding head's feed speed is depicted in Fig. 15, and the other corresponding grinding parameter settings are listed in Table 6. In Fig. 15, with the increase of the grinding head's feed speed, the surface residual stress increases slowly, and the fitting degree of the simulation curve and the experimental curve is higher after correction.

- (3) Analysis of the relationship between residual stress and grinding depth

The surface residual stress after correction is arranged according to the grinding depth is depicted in Fig. 16, and the other corresponding grinding parameter settings are listed in Table 6. In Fig. 16, with the increase of the grinding depth, the surface residual stress increases slowly. The fitting degree of the simulation curve and the experimental curve is higher after correction.

Through the above comparison, it can be found that the simulation results after correction are not much different from the experiment results, and the maximum error is about 22 MPa, which is almost negligible. The above analysis shows that the simulation model after correction can better characterize the variation of ABG residual stress of titanium alloy material and verify the effectiveness of the mathematical model of residual stress after correction.

### 5.3 Precision analysis of molecular dynamics prediction and simulation of titanium alloy thin-walled parts

Through the analysis in Section 6.2, it can be known that the corrected residual stress simulation values agree well with the experiment values. Therefore, more sets of grinding parameters of residual stress are simulated and predicted. Among them, the range of abrasive belt speed is 8–24 m/s, the range of feed speed of grinding head is 0.3–0.9 m/min, and the range of grinding

depth is 0.2–0.6 mm. Each grinding parameter is divided into 20 groups, and  $20^3$  sets of predictions are made. The residual stress prediction results are depicted in Fig. 17. In Fig. 17, the change of the residual stress of the adjacent group naturally transitions without abrupt changes or errors. Within the range of grinding parameters, the larger the feed speed of grinding head and grinding depth, the smaller the abrasive belt speed, the larger the residual stress value obtained; the smaller the feed speed of grinding head and grinding depth, the larger the abrasive belt speed, the smaller the residual stress value obtained. Therefore, in the actual titanium alloy ABG experiment, you can choose a lower feed speed of grinding head and grinding depth and a larger abrasive belt speed to reduce the surface residual stress.

To improve the comparability of simulation results and experiment results, the precision analysis of molecular dynamics simulation is carried out for titanium alloy thin-walled parts. The comparison results are depicted in Fig. 18.

The error comparison between the residual stress simulation results on the surface before and after correction and the experiment results is depicted in Fig. 18. In Fig. 18, the error rate of the corrected residual stress is obviously lower than that before the correction. In Fig. 18a, the residual stress simulation values distribution is relatively concentrated before the correction, all of which range from  $-220$  to  $-260$  MPa. The maximum error rate with the experiment values is 31.05%, and the average error rate is 15.01%. There are two reasons. One is that the influence of grinding heat on residual stress is ignored in the calculation process, which leads to a large deviation; the other is that limited by the computer performance, the algorithm has fewer cycle steps, and it is unable to fully calculate the model, resulting in the lack of divergence between the data, which presents a more centralized state. From Fig. 18b, it can be seen that after correction, the trend of the simulation values is consistent with the experiment values, the maximum error rate of simulation values and experiment values of surface residual stress is reduced to 8.95%, and the average error rate is reduced to 4.44%, which proves the effectiveness of the corrected mathematical model and can effectively predict the surface residual stress after machining.

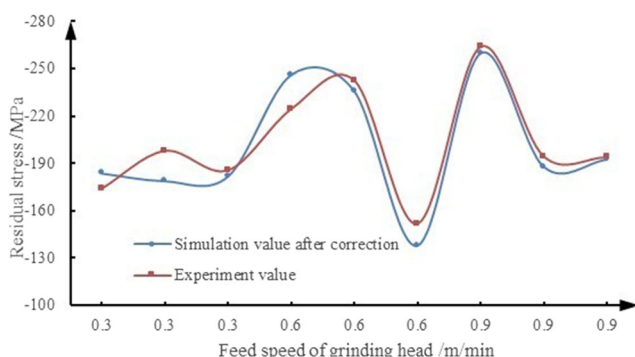


**Fig. 15** Relationship between residual stress and feed speed of grinding head after correction

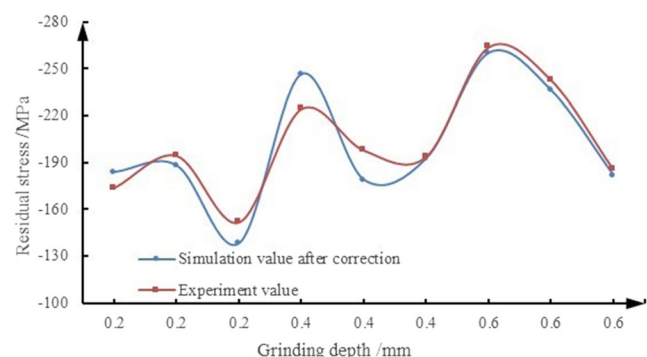


**Fig. 16** Relationship between residual stress and grinding depth after correction.

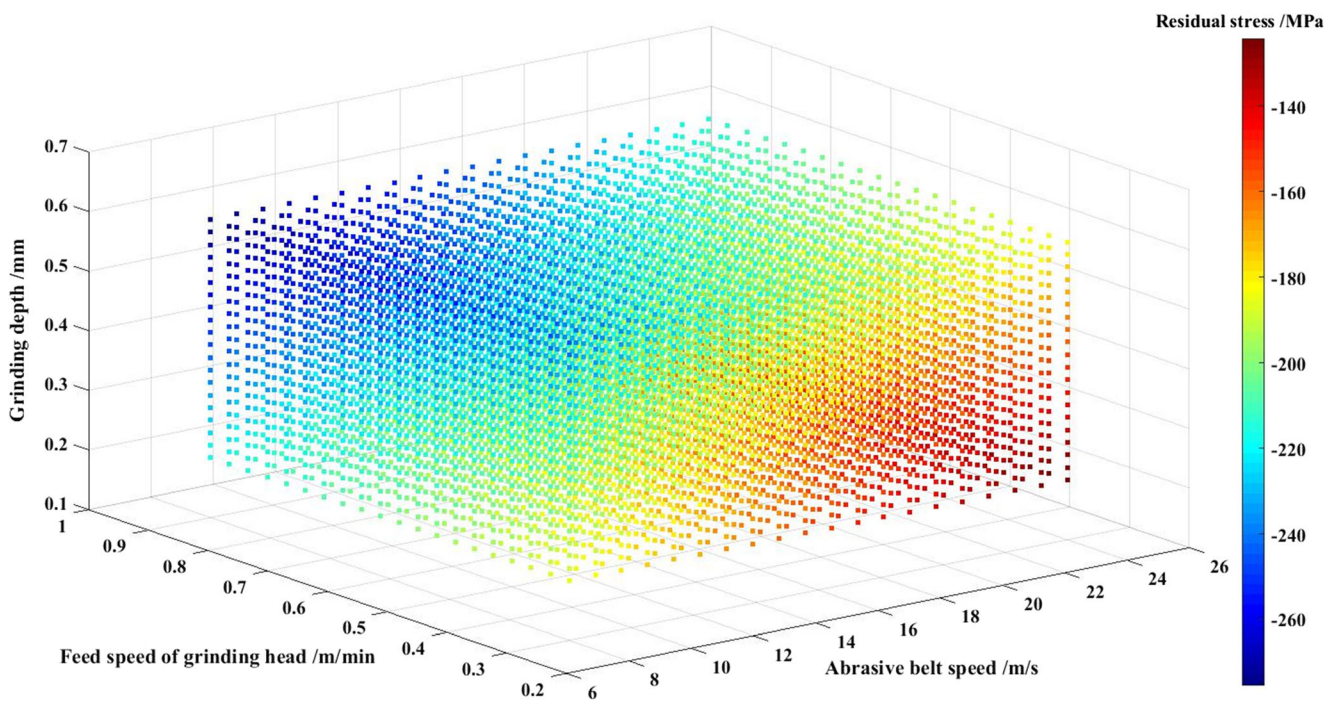


Fig. 17 Prediction of residual stress under  $20^3$  grinding parameters

### 6 Conclusions

Based on the molecular dynamics analysis of titanium alloy ABG, the residual stress simulation of titanium alloy thin-walled parts in ABG is carried out, and the ABG experiment verification of titanium alloy thin-walled parts is developed. In the last, the accuracy analysis of molecular dynamics simulation of titanium alloy thin-walled parts is carried out. The conclusions are as follows:

- (1) The physical model of the titanium alloy ABG molecular system is established, and the molecular 3D model is converted into a planar two-dimensional molecular model system.
- (2) Combined with the residual stress expression model, the characterization of surface residual stress is realized, and the thermal correction coefficient is proposed to modify the simulation model.
- (3) The surface residual stress of the molecular system is simulated and analyzed by using MATLAB. The simulation results agree well with the experiment results.
- (4) Due to the influence of grinding heat, the error rate between simulation values and experiment values is high. After correction, the maximum error rate of surface residual stress is reduced to 8.95%, and the average error rate is reduced to 4.44%.

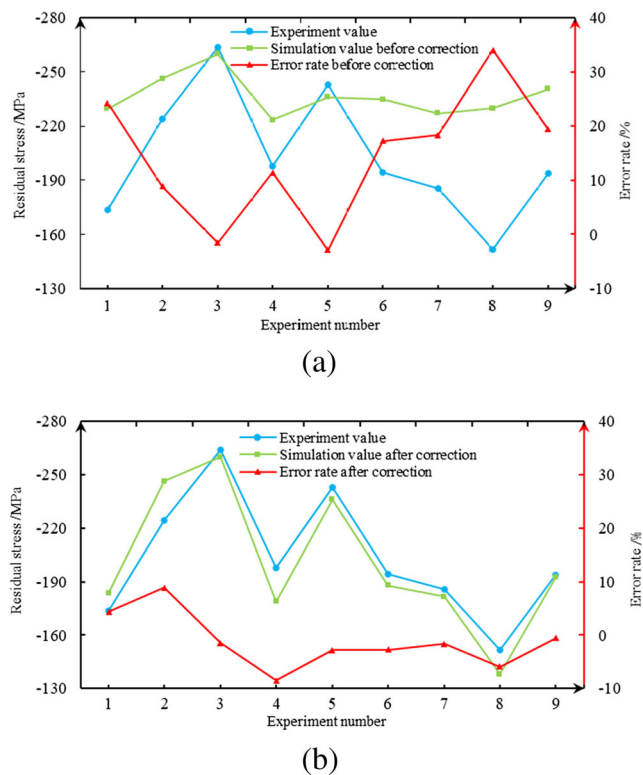


Fig. 18 Comparison of error rate between simulation results and experiment results. (a) Residual stress and error rate before correction. (b) Residual stress and error rate after correction

**Author contribution** Guijian Xiao: funding acquisition, project administration, resources, and supervision. Kangkang Song: investigation, methodology, and writing original draft. Yi He: data curation and software. Wenxi Wang: experiment and conceptualization. Youdong Zhang: writing review and editing. Wentao Dai: validation and visualization.

**Funding** This work was supported by the National Natural Science Foundation of China [Grant No. U1908232]; the National Science and Technology Major Project [Grant No. 2017-VII-0002-0095]; the Funded by China Postdoctoral Science Foundation [Grant No. 2020M673126]; and the Graduate scientific research and innovation foundation of Chongqing [Grant No.CYB20009].

**Data availability** The datasets used or analyzed during the current study are available from the corresponding author on reasonable request.

## Declarations

**Ethical approval** Ethical approval was not required for this study.

**Consent to participate** Written informed consent was obtained from individual or guardian participants.

**Consent to publish** The manuscript was approved by all authors for publication.

**Competing interests** The authors declare no competing interests.

## References

- Xi X, Ding W, Wu Z, Anggei L (2020) Performance evaluation of creep feed grinding of  $\gamma$ -TiAl intermetallics with electroplated diamond wheels. *Chin J Aeronaut* 34:100–109. <https://doi.org/10.1016/j.cja.2020.04.031>
- Huang Y, He S, Xiao G, Li W, Jiahua S, Wang W (2020) Effects research on theoretical-modelling based suppression of the contact flutter in blisk belt grinding. *J Manuf Process* 54:309–317. <https://doi.org/10.1016/j.jmapro.2020.03.021>
- Xiao G, He Y, Huang Y, He S, Wang W, Wu Y (2020) Bionic microstructure on titanium alloy blade with belt grinding and its drag reduction performance. *Proc Inst Mech Eng B J Eng Manuf*. <https://doi.org/10.1177/0954405420949744>
- Fan W, Wang W, Wang J, Zhang X, Qian C, Ma T (2020) Microscopic contact pressure and material removal modeling in rail grinding using abrasive belt. *Proc Inst Mech Eng B J Eng Manuf* 235:3–12. <https://doi.org/10.1177/0954405420932419>
- Miao Q, Ding W, Kuang W, Yang C (2019) Grinding force and surface quality in creep feed profile grinding of turbine blade root of nickel-based superalloy with microcrystalline alumina abrasive wheels. *Chin J Aeronaut* 34:576–585. <https://doi.org/10.1016/j.cja.2019.11.006>
- Xie H, W-l L, Zhu D-h, Z-p Y, Ding H (2020) A systematic model of machining error reduction in robotic grinding. *IEEE/ASME Trans Mechatron* 99:1–11. <https://doi.org/10.1109/TMECH.2020.2999928>
- Wang G, Li W-l, Jiang C, Zhu D-h, Xie H, Liu X-j, Ding H (2021) Simultaneous calibration of multicoordinates for a dual-robot system by solving the AXB = YCZ problem. *IEEE Trans Robot* 1-14. doi:<https://doi.org/10.1109/tro.2020.3043688>
- Rami A, Kallel A, Djemaa S, Mabrouki T, Sghaier S, Hamdi H (2018) Numerical assessment of residual stresses induced by combining turning-burnishing (CoTuB) process of AISI 4140 steel using 3D simulation based on a mixed approach. *Int J Adv Manuf Technol* 97(5-8):1897–1912. <https://doi.org/10.1007/s00170-018-2086-7>
- Nikam SH, Jain NK (2019) Modeling and prediction of residual stresses in additive layer manufacturing by microplasma transferred arc process using finite element simulation. *J Manuf Sci Eng* 141(6). <https://doi.org/10.1115/1.4043264>
- Sasaki T, Yoshida S, Ogawa T, Shitaka J, McGibboney C (2019) Effect of residual stress on thermal deformation behavior. *Materials (Basel)* 12(24). <https://doi.org/10.3390/ma12244141>
- Choi H, Yoon JW, Kwon YN, Seong D (2019) Evolution of residual stress distortion of a machined product for AA7085. *Prod Eng* 13(2):123–131. <https://doi.org/10.1007/s11740-019-00880-9>
- Numerical simulation of dissimilar weld joint in SYSWELD simulation software (2017). *Tehnicky vjesnik - Technical Gazette* 24 (Supplement 1). doi:<https://doi.org/10.17559/tv-20150513074103>
- Darmadi D (2019) Incorporating aged martensite model in residual stress prediction of ferritic steels girth weld. *FME Trans* 47(4):901–913. <https://doi.org/10.5937/fmet1904901D>
- Wang F, Mao K, Li B (2018) Prediction of residual stress fields from surface stress measurements. *Int J Mech Sci* 140:68–82. <https://doi.org/10.1016/j.ijmecsci.2018.02.043>
- Sun C, Xiu S, Hong Y, Kong X, Lu Y (2020) Prediction on residual stress with mechanical-thermal and transformation coupled in DGH. *Int J Mech Sci* 179:105629. <https://doi.org/10.1016/j.ijmecsci.2020.105629>
- Valiček J, Czán A, Harničárová M, Šajgalík M, Kušnerová M, Czánová T, Kopal I, Gombár M, Kmec J, Šafář M (2019) A new way of identifying, predicting and regulating residual stress after chip-forming machining. *Int J Mech Sci* 155:343–359. <https://doi.org/10.1016/j.ijmecsci.2019.03.007>
- Lu Y, Pan Z, Bocchini P, Garmestani H, Liang S (2019) Grain size sensitive-MTS model for Ti-6Al-4V machining force and residual stress prediction. *Int J Adv Manuf Technol* 102(5-8):2173–2181. <https://doi.org/10.1007/s00170-019-03309-w>
- Pan Z, Feng Y, Ji X, Liang SY (2017) Turning induced residual stress prediction of AISI 4130 considering dynamic recrystallization. *Mach Sci Technol* 22(3):507–521. <https://doi.org/10.1080/10910344.2017.1365900>
- Fergani O, Jiang X, Shao Y, Welo T, Yang J, Liang S (2015) Prediction of residual stress regeneration in multi-pass milling. *Int J Adv Manuf Technol* 83(5-8):1153–1160. <https://doi.org/10.1007/s00170-015-7464-9>
- Zheng B, Yu H, Lai X, Lin Z (2016) Analysis of residual stresses induced by riveting process and fatigue life prediction. *J Aircr* 53(5):1431–1438. <https://doi.org/10.2514/1.C033715>
- Shan C, Zhang M, Zhang S, Dang J (2020) Prediction of machining-induced residual stress in orthogonal cutting of Ti6Al4V. *Int J Adv Manuf Technol* 107(5-6):2375–2385. <https://doi.org/10.1007/s00170-020-05181-5>
- Ling H, Yang C, Feng S, Lu H (2020) Predictive model of grinding residual stress for linear guideway considering straightening history. *Int J Mech Sci* 176:105536. <https://doi.org/10.1016/j.ijmecsci.2020.105536>
- Doan D-Q, Fang T-H, Tran A-S, Chen T-H (2019) Residual stress and elastic recovery of imprinted Cu-Zr metallic glass films using

- molecular dynamic simulation. *Comput Mater Sci* 170:109162. <https://doi.org/10.1016/j.commatsci.2019.109162>
24. Zhou XW, Wadley HN, Johnson RA, Larson DJ, Tabat N, Cerezo A, Petford-Long AK, Smith GDW (2001) Atomic scale structure of sputtered metal multilayers. *Acta Mater* 49(19):4005–4015. [https://doi.org/10.1016/S1359-6454\(01\)00287-7](https://doi.org/10.1016/S1359-6454(01)00287-7)
25. Zhou M (2003) A new look at the atomic level virial stress: on continuum-molecular system equivalence. *Proc R Society A: Mathematical, Physical and Engineering Sciences* 459(2037): 2347–2392. [https://doi.org/10.1016/S1359-6454\(01\)00287-7](https://doi.org/10.1016/S1359-6454(01)00287-7)
26. Zhang Y, Zhang W, Guo G (2011) Finite element thermal model and experimental verification for constant pressure belt grinding process. *J Sichuan Univ (Engineering Science Edition)* 43:238–242+247. <https://doi.org/10.15961/j.jsuese.2011.06.013>
27. He Y, Xiao G, Li W, Huang Y (2018) Residual stress of a TC17 titanium alloy after belt grinding and its impact on the fatigue life. *Materials* 11(11):221801–221816. <https://doi.org/10.3390/ma11112218>

**Publisher's note** Springer Nature remains neutral with regard to jurisdictional claims in published maps and institutional affiliations.